Implications of a zero-nonlinearity wavelength in photonic crystal fibers doped with silver nanoparticles

Surajit Bose, Ambaresh Sahoo, Rik Chattopadhyay, Samudra Roy, Shyamal K. Bhadra, and Govind P. Agrawal

Phys. Rev. A **94**, 043835 — Published 19 October 2016

DOI: 10.1103/PhysRevA.94.043835

Implications of a zero-nonlinearity wavelength in photonic crystal fibers doped with silver nanoparticles

Surajit Bose,[1,2,*] Ambaresh Sahoo,[3] Rik Chattopadhyay,[1] Samudra Roy,[3] Shyamal K. Bhadra,[1,2,†] and Govind P. Agrawal[4]

[1]*Fiber optics and Photonics Division, CSIR-Central Glass and Ceramic Research Institute (CGCRI),196 Raja S.C. Mullick Road, Kolkata-700032, India*

[2]*Academy of Scientific and Innovative Research (AcSIR), CGCRI, India*

[3]*Department of Physics, Indian Institute of Technology Kharagpur, Kharagpur-721302, India*

[4]*The Institute of Optics, University of Rochester, Rochester, New York 14627, USA*

e-mail address: [*]*surajitbose@cgcri.res.in,* [†]*skbhadra@cgcri.res.in*

Photonic crystal fibers doped with silver nanoparticles exhibit a Kerr nonlinearity that can be positive or negative depending on the input wavelength and vanishes at a specific wavelength. The existence of negative nonlinearity allows soliton formation even in the normal-dispersion region of the fiber, and the zero-nonlinearity wavelength (ZNW) acts as a barrier for the Raman-induced red shift of solitons. We adopted variational principle to understand the role of zero-nonlinearity point on Raman red-shift and verified its prediction numerically for fundamental and higher-order solitons. We show how the simultaneous presence of a ZNW and a zero-dispersion wavelength affects soliton evolution inside such fibers and find a number of unique features like the position and the spectral bandwidth of the dispersive wave that change with the location of the ZNW.

PACS number(s):42.65.Tg, 42.65.Wi, 42.65. Re

I. INTRODUCTION

Study of nonlinear phenomena in optical fibers has been an active area of research, both from the fundamental and application perspectives [1-15]. It is well known that optical pulses can propagate as solitons by balancing the effects of group-velocity dispersion (GVD) through self-phase modulation induced by the Kerr nonlinearity [2]. Photonic crystal fibers (PCFs) have an added advantage over conventional optical fibers as they offer endlessly single mode behavior and an easy dispersion tailoring with enhanced nonlinearity [3-5]. Solitons react to the presence of higher-order dispersion by generating dispersive waves (DWs) that play a pivotal role in supercontinuum generation when short optical pulses propagate inside PCFs [6-8]. Evolution of such pulses inside a PCF with more than one zero-dispersion wavelength (ZDW) leads to fascinating effects such as suppression of the Raman-induced frequency shift (RIFS) [9-11], controllable RIFS in nonlinear metamaterials [12], a blue shift of solitons [13], and all-optical control of GVD [14-15]. In all these cases the formation of optical solitons required anomalous dispersion because most optical fibers exhibit a positive Kerr nonlinearity ($n_2 > 0$) at all wavelengths.

Recent work has shown that PCFs whose core is doped with metal nanoparticles exhibit n_2 that varies rapidly with wavelength and can even change sign at a specific wavelength [16-18]. The existence of a zero-nonlinearity wavelength (ZNW) is intriguing since such PCFs can exhibit both a ZNW and a ZDW that do not coincide, making it possible to realize four spectral regions with different signs of the GVD parameter β_2 and the Kerr parameter n_2. In this work we study numerically the propagation of short optical pulses inside silver-doped PCFs. By focusing on the wavelength dependence of n_2 and tailoring the ZNW, we discover new physics. In particular, we find that, ZNW suppresses the spectral red shift arising from Raman scattering. We adopt a variational technique where the frequency dependent higher-order nonlinear term acts as a perturbation. In this entire work our emphasis is on understanding the role of the ZNW on the evolution of pulse spectrum.

This paper is organized as follows. In section II, we introduce the simple design of the doped PCF exhibiting negative nonlinearity and for that generalized nonlinear Schrödinger equation (GNLSE) is formulated. In Sec. III, we adopt the variational method to explain the restriction of Raman red-shift due to ZNW. In section IV, we numerically study the evolution of higher order solitons when ZDW and ZNW are present in the system simultaneously. Section V focuses on the graphical examination of how the variation of doping concentration changes the ZNW which changes the position and the

bandwidth of DW as described in Sec. IV. Finally in Sec. VI, we conclude our findings.

II. GNLSE FOR A SILVER-DOPED FIBER

We consider a PCF in the form of a solid-core microstructure optical fiber shown in Fig. 1. Its silica core is doped with silver nanoparticles. The pitch of air holes surrounding the core of the PCF is $3\mu m$ with an air-filling fraction of 0.9. Geometrical parameters of the fibre are selected from the fabrication point of view.

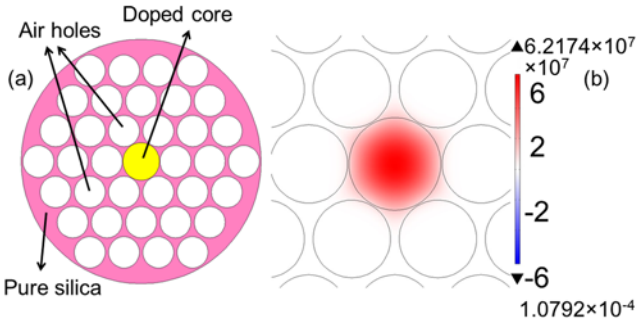

FIG. 1. (Color online) (a) Schematic cross-section of the proposed fiber. (b) Fundamental mode field distribution calculated at the operating wavelength of 880 nm.

Before proceeding it is important to modify the standard GNLSE for doped PCFs [1] for which the Kerr nonlinearity changes rapidly with wavelength. In our previous work [18] we assumed that both Kerr and Raman parts were affected by the silver nanoparticles. This led to Raman-induced spectral blue shifts that appeared to be nonphysical. In this work, we assume that silver nanoparticles do not affect the Raman contribution to the fiber nonlinearity and write the nonlinear polarization in the form,

$$P_{NL}(\vec{r},t)=\frac{3\varepsilon_0}{4}[(1-f_R)\chi_{eff}^{(3)}\left|\mathcal{E}(\vec{r},t)\right|^2\mathcal{E}(\vec{r},t) + f_R\chi_h^{(3)}\mathcal{E}(\vec{r},t)\int_{-\infty}^{t}h_R(t-\tau)\left|\mathcal{E}(\vec{r},t)\right|^2 d\tau] \quad (1)$$

Where $\mathcal{E}(\vec{r},t)=\mathrm{F}(x,y)\,A(z,t)\exp(\mathrm{i}\beta_0 z)$ is the total electric field containing the spatial distribution $F(x, y)$ and time-domain envelope function $A(z,t)$. Here f_R the fractional Raman contribution, $\chi_{eff}^{(3)}$ is the effective third-order susceptibility in the presence of metal nanoparticles and $\chi_h^{(3)}$ is the third-order susceptibility of host glass. Using this expression of nonlinear polarization and under slowly varying envelope approximation, the GNLSE takes the following form [1].

$$\frac{\partial A}{\partial z}-i\sum_{n=1}^{\infty}\frac{\beta_n}{n!}\left(i\frac{\partial}{\partial t}\right)^n A=i(1-f_R)\gamma_{eff}\left|A(z,t)\right|^2A(z,t)+ if_R\gamma A(z,t)\int_0^{\infty}h_R(t')\left|A(z,t-t')\right|^2dt' \quad (2)$$

β_n is the n^{th} order dispersion parameter. Both $\gamma(\omega)\approx\gamma_0+\gamma_1(\omega-\omega_0)$ and $\gamma_{eff}(\omega)$ are frequency dependent nonlinear coefficients of the undoped and the doped PCF defined as,

$$\gamma_0=\frac{2\pi n_2}{\lambda_0 A_{eff}},\ \gamma_{eff}=\frac{2\pi\,\mathrm{Re}(n_{2eff})}{\lambda_0 A_{eff}},\ \gamma_1\approx\frac{\gamma_0}{\omega_0},\ n_2=\frac{3\chi_h^{(3)}}{4\varepsilon_0 c}$$

$$n_{2eff}=\frac{3\chi_{eff}^{(3)}}{4\varepsilon_0 c\varepsilon_{eff}}.$$

Here $\varepsilon_{eff}=\frac{\varepsilon_h(1+2\sigma f)}{(1-\sigma f)}$ with $\sigma=\frac{\varepsilon_i-\varepsilon_h}{\varepsilon_i+2\varepsilon_h}$ is the effective permittivity of the silver-doped PCF calculated from Maxwell-Garnett theory [19]. The filling factor f is the volume fraction of the silver nano-metric inclusions. Further, ε_i and ε_h are the dielectric functions of silver [20] and silica, respectively.

The effective third-order susceptibility of silver-doped fibers has been calculated using theory of composite nonlinear materials [21] and is given by [18]

$$\chi_{eff}^{(3)}=f\frac{\chi_i}{\left|B\right|^2B^2}+\chi_h\frac{D}{\left|1-f\sigma\right|^2(1-f\sigma)^2} \quad (3)$$

$$B=\frac{(1-\sigma f)(\varepsilon_i+2\varepsilon_h)}{3\varepsilon_h} \quad (4)$$

$$D=1-f\left\{1-0.4(4\sigma^2\left|\sigma\right|^2+3\sigma\left|\sigma\right|^2+\sigma^3+9\left|\sigma\right|^2+9\sigma^2)\right\} \quad (5)$$

The susceptibility of host silica glass and silver are $\chi_h=2.233\times10^{-22}m^2/V^2$ and $\chi_i=(-6.3+i1.9)\times10^{-16}m^2/V^2$ respectively.

Dispersion and the nonlinear parameters of the fiber shown in Fig. 1 are calculated using the finite element method (FEM) using a filling factor of $f=6\times10^{-3}$. At the pump wavelength of $\lambda_0=880nm$ we found $\beta_2=0.0297\,ps^2/m$, $\gamma_0=0.040W^{-1}m^{-1}$, $\gamma_1\approx0.0186W^{-1}m^{-1}fs$. Frequency dependence of γ_{eff} is included using $\gamma_{eff}(\omega)=\gamma_{0eff}(\omega_0)+\gamma_{1eff}(\omega-\omega_0)$ with $\gamma_{0eff}=-0.5334W^{-1}m^{-1}$ and $\gamma_{1eff}\approx-0.925W^{-1}m^{-1}fs$ for the chosen value of f. The ZDW and ZNW of the PCF are found to be at 1023 nm and 1205 nm respectively.

III. RESTRICTION OF RAMAN RED-SHIFT DUE TO ZNW

In this section we try to understand the effect of ZNW on pulse dynamics. We adopt the standard variational method [22] and treat the higher-order nonlinear terms resulting from Taylor-series expansion of the frequency dependent nonlinearity as a perturbation. The GNLSE as given in Eq. (2) can be written in a normalized form as,

$$\frac{\partial u}{\partial \xi} = -\frac{i}{2}\mathrm{sgn}(\beta_2)\frac{\partial^2 u}{\partial \tau^2} + \sum_{n=3}^{\infty} i^{n+1}\delta_n \frac{\partial^n u}{\partial \tau^n} + iN^2\,\mathrm{sgn}(\gamma_{0eff})(1-f_R)|u|^2 u + iN^2\left[\begin{array}{l}\sum_{m=1}^{\infty} i^m \mu_{meff}(1-f_R)\frac{\partial^m}{\partial \tau^m}(|u|^2 u) \\ +\Gamma f_R |u|^2 u - \Gamma \tau_R u \frac{\partial |u|^2}{\partial \tau} + i\Gamma s f_R \frac{\partial}{\partial \tau}(|u|^2 u)\end{array}\right] \quad (6)$$

where the parameters are rescaled as,

$u = AP_0^{-1/2}$, $\mu_{meff} = \dfrac{\gamma_{meff}}{m!\left|\gamma_{0eff}\right| T_0{}^m}$, $\delta_n = \dfrac{\beta_n}{n!\left|\beta_2\right| T_0^{n-2}}$,

$\Gamma = \dfrac{\gamma_0}{\left|\gamma_{0eff}\right|}$, $\xi = \dfrac{z}{L_D}$, $L_D = \dfrac{T_0^2}{\left|\beta_2\right|}$, $L_{NL} = \dfrac{1}{\left|\gamma_{0eff}\right| P_0}$, $N^2 = \dfrac{L_D}{L_{NL}}$,

$\tau = \dfrac{t - z v_g^{-1}}{T_0} = \dfrac{T}{T_0}$, $\tau_R = \dfrac{T_R}{T_0}$, $s = \dfrac{1}{\omega_0 T_0}$. Here, P_0 , T_0 and v_g are the input peak power, initial pulse width and the group velocity of the pulse respectively.

To study the impact of ZNW, we adopt the soliton perturbation analysis treating Eq. (6) as a perturbed NLSE:

$$i\frac{\partial u}{\partial \xi} - \frac{1}{2}\mathrm{sgn}(\beta_2)\frac{\partial^2 u}{\partial \tau^2} + \mathrm{sgn}(\gamma_{0eff})|u|^2 u = i\Delta(u) \quad (7)$$

Where $\Delta(u)$ contains all first-order perturbation terms:

$$\Delta(u) = -i\tau_R \Gamma u \frac{\partial}{\partial \tau}|u|^2 - \left(\mu_{1eff}(1-f_R) + \Gamma s f_R\right)\frac{\partial}{\partial \tau}\left(|u|^2 u\right) + i\left(\Gamma - \mathrm{sgn}(\gamma_{0eff})\right) f_R |u|^2 u \quad (8)$$

The perturbative theory is developed by introducing the ansatz,

$$u(\xi,\tau) = \left(\frac{E(\xi)\eta(\xi)}{2}\right)^{1/2} \mathrm{sech}\left[\eta(\xi)\left(\tau - q(\xi)\right)\right] \exp\left[i\phi(\xi) - i\Omega(\xi)\left(\tau - q(\xi)\right) - i\kappa(\xi)\left(\tau - q(\xi)\right)^2\right] \quad (9)$$

where all six normalised parameters energy E , amplitude η, temporal position q , phase ϕ, frequency shift Ω and chirp κ are dimensionless which are functions of propagation distance ξ. Using the standard Lagrangian density and integrating it over the time parameter τ we get the total Lagrangian in the form,

$$L = -\left[\phi_\xi E + \Omega q_\xi E - \frac{\pi^2 \kappa_\xi E}{12\eta^2}\right] + \frac{E^2\eta}{6} - \frac{1}{2}\left[\frac{1}{3}E\eta^2 + \Omega^2 E + \frac{\pi^2 E\kappa^2}{3\eta^2}\right] + i\int_{-\infty}^{\infty}\left(\Delta^* u - \Delta u^*\right)d\tau \quad (10)$$

This normalized Lagrangian lead to a set of ordinary differential equations for the six parameters that describe the soliton dynamics. Exploiting the perturbation $\Delta(u)$ and denoting the ξ derivative with a subscript, four of these equations are

$$E_\xi = 0 \quad (11)$$

$$\eta_\xi = 2\kappa\eta \quad (12)$$

$$\Omega_\xi = -\frac{4}{15}\tau_R \Gamma E\eta^3 + \frac{2}{3}\mu_{1eff}(1-f_R)E\eta\kappa + \frac{2}{3}\Gamma s f_R E\eta\kappa \quad (13)$$

$$\kappa_\xi = 2\kappa^2 + \frac{\eta^3}{\pi^2}\left[E - 2\eta + E\Omega\mu_{1eff}\left(1-f_R\right) + Es\Omega\Gamma f_R + \left(\Gamma - \mathrm{sgn}\left(\gamma_{0eff}\right)\right) f_R E\right] \quad (14)$$

The equation for Ω is the most relevant for us as it describes changes in the soliton frequency with distance. The first term in Eq. (13) corresponds to the standard RIFS. The presence of the second term containing μ_{1eff} shows that RIFS is reduced by the presence of a ZNW. Note that we omitted the third order dispersion (TOD) effects in this calculation to capture the sole effect of ZNW on pulse dynamics.

To compare the variational predictions with the full GNLSE, we solved numerically Eq. (6) using parameters $T_0 = 50\,fs$; $\lambda_0 = 880\,nm$; $\beta_2 = 0.0297\,ps^2/m$; and $\beta_{n>2} = 0$; $\gamma_0 = 0.040 W^{-1}m^{-1}$; $\gamma_{0eff} = -0.5334 W^{-1}m^{-1}$ and $\gamma_{1eff} = (\pm 1, 0)\times 0.925 W^{-1}m^{-1}fs$. The value and numeric sign of γ_{1eff} control the location of the ZNW and slope of the nonlinear dispersion, respectively. In Fig. 2(a) and 2(b) we show the evolution of a second-order soliton $(N = 2)$ in the presence and absence of the ZNW. In the absence of ZNW, Raman soliton accelerates and its spectrum shifts considerably toward the red side as shown by an arrow in Fig. 2(b). This shift is reduced significantly when a ZNW is present [vertical dotted line in Figs. 2(a) and 2(b)]. The temporal shift is also reduced because of a reduced RIFS. Variational treatment also shows that the RIFS is reduced in presence of ZNW. We solve the coupled differential equations given as Eq. (11-14) and plot the evolution of soliton's frequency shift Ω with distance in Fig. 2(c). Three curves correspond to three different values of the parameter μ_{1eff}. The middle curve is for $\mu_{1eff} = 0$ which implies no ZNW. The other two curves show that the RIFS becomes less (more) when the numeric sign of μ_{1eff} is

negative (positive). As a final check, we solve Eq. (6) numerically for a fundamental ($N=1$) soliton and find the reduced RIFS as shown in Fig. 2(d). Here we must emphasize that a major approximation in variational method is the preservation of pulse shape. Because of this constrain we are forced to use $N=1$ for which the changes in the RIFS are relatively small. However, even for $N=1$ the RIFS reduction is evident in Fig. 2(d). Moreover, the variational predictions agree with the numerical data shown in Fig. 2 (c) by blue squares. We conclude that the variational method qualitatively describes how the interplay between the ZNW and accumulated chirp on the pulse limits the extent of RIFS.

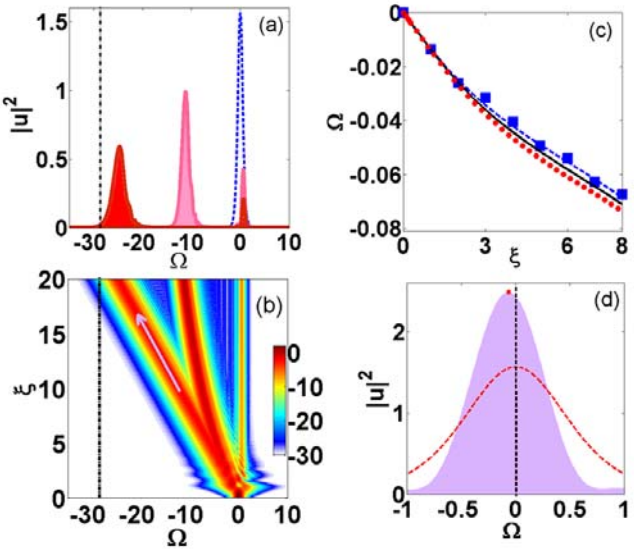

FIG. 2. (Color online) (a) Raman-induced spectral shift at $\xi=20$ of a second-order soliton ($N=2$) in the absence (red pulse) (dark grey pulse) and presence (pink pulse) (light grey pulse) of a ZNW. (b) Spectral evolution inside the PCF in the two cases. The arrow marks the absence of a ZNW. (c) Frequency shifts with distance as predicted by the variational technique for $N=1$; blue squares represents numerical data that agrees with the dashed blue line. Dashed blue line (upper) represents the negative higher order nonlinear coefficient and dotted red line represents the positive higher order nonlinear coefficient. Black solid line (middle) indicates absence of higher order nonlinear coefficient. (d) Variational prediction comparing soliton spectrum at a distance of $\xi=8$ with the input spectrum (dotted curve). Red dot at the peak shows the extent of RIFS.

IV. HIGHER ORDER SOLITONS AND DISPERSIVE WAVES

In this section we study how a higher-order soliton is influenced by the ZDW and ZNW when both are present simultaneously. To simulate the soliton dynamics inside adopted PCF, we solved Eq. (1) to (5) numerically. Figure 3(c) shows wavelength dependence of β_2 and γ_{eff} for a silver-doped PCF with $\gamma_{1eff}\approx -0.694 W^{-1}m^{-1}fs$ so that ZNW is 1374 nm. For numerical simulations we expand the frequency dependent nonlinear parameter in a Taylor series and retain the linear term, which is a reasonable approximation in the spectral range of 800-1300 nm. We checked our results by solving Eq. (2) in the frequency domain, and the results were almost identical.

Numerical simulations are performed for the input pulse shape, $A(0,t)=A_0\,\mathrm{sech}\left(T/T_0\right)$ with $T_0=50\,fs$. The peak power ($P_0=A_0^2$) of 200W is chosen such that $N=\dfrac{|\gamma_{0eff}|P_0T_0^2}{|\beta_2|}\approx 3$ at the input wavelength of 880 nm. In this case as shown in Fig 3(c), the optical pulse encounters three distinct propagation regions: region (1) is solitonic ($\beta_2>0,\gamma_{eff}<0$), region (2) ($\beta_2<0,\gamma_{eff}<0$) is non-solitonic and region (3) is again solitonic with ($\beta_2<0,\gamma_{eff}>0$).

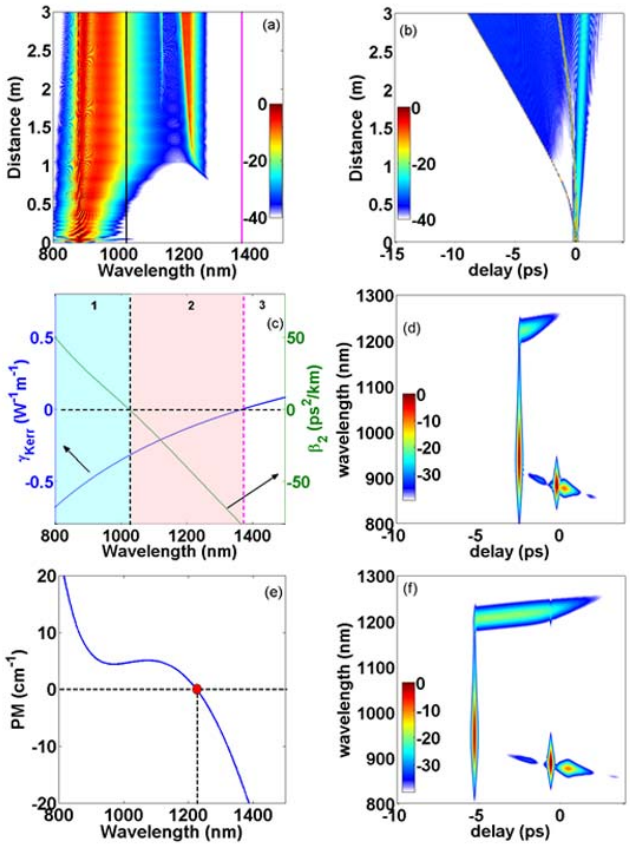

FIG. 3. (Color online) Spectral (a) and temporal (b) evolution of the pulse over 3 m. Black and red vertical lines in (a) mark the ZDW (1023nm) and the ZNW (1374 nm), respectively (c) GVD and nonlinear profiles of the PCF as a function of wavelength. (d)

Spectrogram at 1.2 m where DW initiates. (e) Phase-matched curve; a red circle indicates the location of DW (f) Spectrogram at 2 m.

We launch the pulse in region 1 so that it begins its evolution as a soliton. Figures 3(a) and 3(b) shows the evolution of a third-order soliton over a 3-m-long PCF whose dispersion and nonlinear profiles are depicted in Fig. 3(c). As expected, pulse spectrum shifts initially toward the red side through RIFS, but the presence of a ZDW (black vertical line) at 1023 nm suppresses RIFS. The dispersive wave radiation emitted due to the presence of ZDW falls in region 2 near 1220 nm. Location of this radiation is obtained analytically from the phase-matching argument [1,23] between the soliton and dispersive wave using

$$\sum_{n\geq 2}\beta_n(\omega-\omega_s)^n=\left[\gamma_{oeff}(\omega_s)+\gamma_{1eff}(\omega-\omega_s)\right]P_s \qquad (15)$$

Here ω_s is the soliton frequency at the onset of the radiation. Position of this frequency is recorded from the spectrogram at 1.2 m length where the radiation initiates in Fig. 3(d). P_s is the peak power of a fundamental soliton formed after the fission process. Dispersion and the nonlinear parameters appearing in Eq. (15) are at the soliton central frequency ω_s. Phase matching curve is plotted in Fig. 3 (e). The predicted frequency of the dispersive wave matches well with simulation.

To understand the pulse dynamics in detail, we show a spectrogram in Fig. 3(f) at a distance of 2 m. The formation of two Raman solitons after the fission process is seen clearly. The spectra of both Raman solitons are red-shifted compared to the input pulse. Their positions are shifted toward negative delay because red-shifted solitons travel faster compared to the input pulse. As soon as the spectrum of the first Raman soliton overlaps with the ZDW, a strong spectral peak appears on the red side of the ZDW around 1220 nm [see Fig. 3(a)]. This peak represents radiation shed by the Raman soliton in the non-solitonic region [region 2 in Fig. 3(c)]. As it is well known [1], spectral recoil from this DW suppresses the RIFS. Exponential amplification of this DW seen in Fig. 3 (a) agrees with the results in [10] where a PCF with two ZDWs was used. In Fig. 3 the ZNW is too far to play a significant role. However, the configuration studied in sec. II gives a ZNW of 1205 nm. In Fig. 4 we show what happens when the ZNW is moved to 1205 nm while keeping all other parameters identical to those in Fig. 3. From the spectral evolution seen in Fig 4 (a), it is clear that the ZNW acts as a barrier. Both the bandwidth and position of the DW change when the location of ZNW changes from 1374 to 1205 nm. Now the radiation initiates at a distance of 1.5 m compared to the previous case where it initiated at 1.2 m. Also, the pulse spectrum hits the ZDW further away. The ZNW pushes the location of DW from 1220 nm to nearly 1177 nm. Location of the DW is cross-checked analytically using Eq. (15). It matches with the simulation quite well. Rest of the pulse dynamics remains nearly the same.

In order to understand how the width of region 2 in Fig. 4 affects soliton evolution, we shift the ZNW to 1135 nm in Fig. 5, while keeping other parameters same. From the spectral evolution seen in Fig 5(a), it is clear that the ZNW acts as a barrier as the spectrum is mostly confined to regions 1 and 2. However, now two distinct DWs are visible in Fig. 5(a) and 5(b). One DW is formed at a distance of 1.3 m and the other around 1.8 m. The spectrogram in Fig. 5(d) shows a weak DW in the region 3 at its original wavelength near 1200 nm. Since this DW lies in the region 3, it is not amplified. Rather, a second much stronger DW is emitted in the spectral region 2 at a distance of 1.8 m when the RIFS is suppressed at the ZDW boundary. The cone shape region on
the left in Fig. 5(b) shows how this DW spreads, traveling faster than the input pulse. The phase-match curve is plotted for the stronger DW in Fig. 5(e). Both the DWs in Fig. 5(f) are clearly visible in the spectrogram at a distance of 2 m. Dark blue wing corresponds to the weak one and the turquoise region to the strong one.

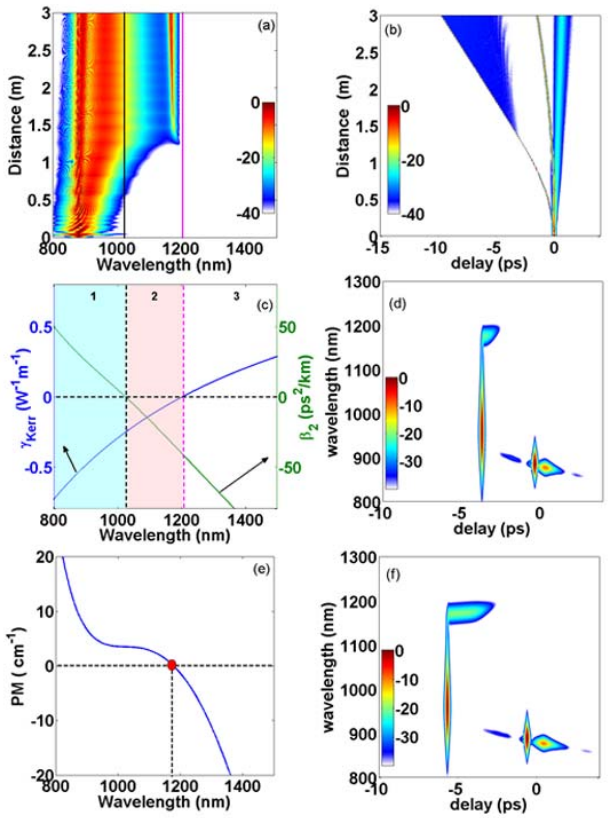

FIG. 4. (Color online) Spectral (a) and temporal (b) evolution of the pulse over 3 m. Black and red vertical lines in (a) mark the ZDW (1023 nm) and the ZNW (1205 nm), respectively (c) GVD and nonlinear profiles of the PCF as a function of wavelength. (d) Spectrogram at 1.5 m. (e) Phase-matching curve; a red circle indicates the wavelength of the DW. (f) Spectrogram at 2 m.

In Fig. 6 we further reduce the region 2 by shifting the ZNW to 1073 nm so that its bandwidth is just 50 nm. All other parameters remain same. The spectral evolution in Fig. 6(a) shows that a DW begins to form near 1180 nm after 1.6 m, but its spectrum blue-shifts toward the ZNW with further propagation. At the same time, the RIFS is no longer blocked by the ZDW, and the Raman soliton occupies the region 2 where solitons are not supposed to form. To understand the underlying physics, we show in Fig. 6(d) to 6(f) three spectrograms at a distance of 1.7 m, 2 m and 3 m respectively. As expected, a weak DW forms at 1.7 m when the spectrum of red-shifted Raman soliton just overlaps the ZDW [Fig. 6 (d)]. We also see that the Raman soliton has trapped this DW and forces it to shift its spectrum through cross-phase modulation. Indeed, at a distance of 2 m, the spectrogram in Fig. 6(e) shows that the DW is dragged by the Raman soliton, whose spectrum is now much wider and ranges from 850 to 1250 nm. At this distance, most of the DW energy is at a wavelength near the ZNW.

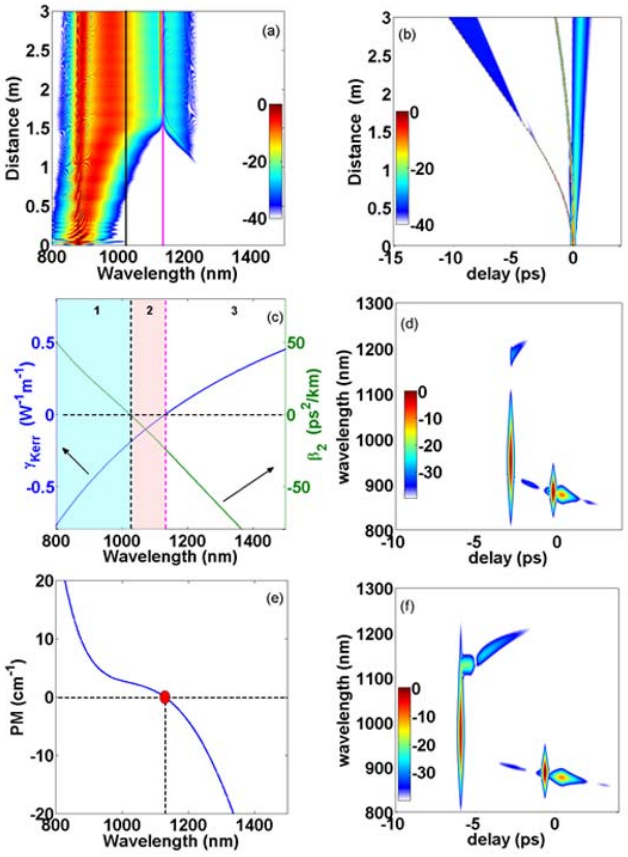

FIG. 5. (Color online) Spectral (a) and temporal (b) evolution over 3 m. Black and red vertical lines in (a) mark the ZDW (1023 nm) and the ZNW (1135 nm), respectively (c) GVD and nonlinear profiles of the PCF. (d) Spectrogram at 1.3 m. (e) Phase-matching curve; a red circle indicates the location of DW. (f) Spectrogram at 2 m.

The spectrogram in Fig. 6 (f) also shows that Raman soliton drags the DW with it even at larger distance (3 m), and both are travelling faster than the original pulse. At this point, the spectrum of DW lies within the broad soliton spectrum. The important conclusion is that, when the region 2 is made narrower by bringing the ZNW closer to the ZDW, Raman soliton can tunnel through it, resulting in a much shorter soliton with a very broad spectrum. At the same time,solitons drags the DW with it.

As a further check, we move the ZNW so close to the ZDW that the two coincide, i.e., the bandwidth of the region 2 has been reduced to zero. The top row of Fig. 7 shows the spectral and temporal evolutions of the pulse in this situation and should be compared with the top row of Fig. 6. The temporal evolutions are quite similar with the main difference that the DW, trapped by the Raman soliton, is much less spread. Figure 7(a) shows that the soliton spectrum is now confined to the region 1 and does not penetrate the ZNW barrier.

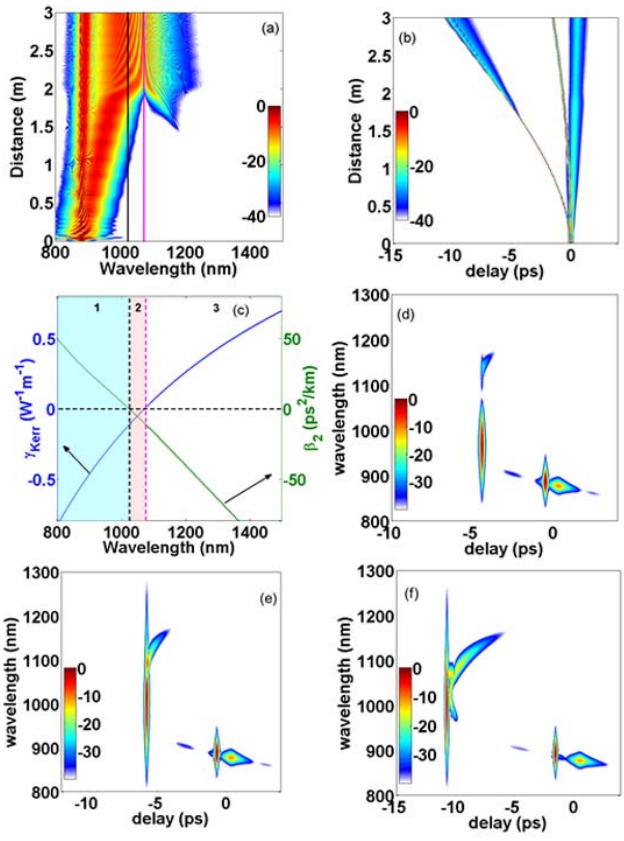

FIG. 6. (Color online) Spectral (a) and temporal (b) evolution over 3m. Black and red vertical lines in (a) mark the ZDW (1023nm) and the ZNW (1073nm), respectively (c) GVD and nonlinear profiles of the PCF. (d), (e) and (f) are the spectrograms corresponding to 1.7 m, 2 m and 3 m. Notice that the DW blue-shifts along the length of the fiber.

It also confirms from the spectrogram at 4 m fiber length in Fig. 7(d), that mostly solitonic energy is not able to overcome the barrier. In contrast, both DWs lie in the region 3 beyond the ZNW.

Finally, we change the dispersive properties of the PCF such that of all higher-order dispersion terms are negligible ($\beta_n = 0$ for $n > 2$). Clearly no ZDW exists for such a fiber. The bottom row of Fig. 7 shows this case by keeping the ZNW still at 1023 nm. From Fig. 7(e) it is evident that the RIFS is reduced, and no DW exists in the region 3 that lies beyond the ZNW. Here ZNW plays the role of a true barrier that restricts the RIFS. This case has already been discussed in sec. III in detail.

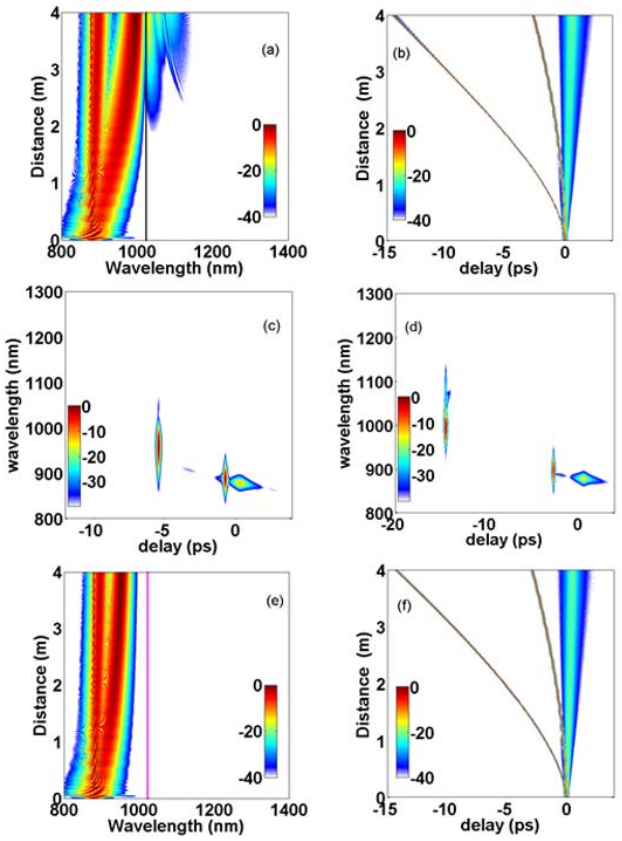

FIG. 7. (Color online) Spectral (a) and temporal (b) evolution when the ZDW and ZNW coincide at 1023 nm. (c) and (d) are the spectrograms at 2 m and 4 m respectively. Fiber dispersion is modified in (e) and (f) such that the ZDW is absent but ZNW coincides at 1023 nm (red vertical line in (e)).

V. CONTROLLING DISPERSIVE WAVES BY TAILORING THE ZNW

In this section we study how the ZNW controls the frequency (or wavelength) of DWs. To see how the presence of ZNW affects the generation of DWs, we plot the DW wavelength λ_{DW} as a function of ZNW in Fig. 8(a) and 8(b) both numerically using Eq. (2) and analytically using Eq. (15). In both cases the analytical predictions match well with the numerical results. From the data in Fig. 8(a) we see that λ_{DW} follows the ZNW almost linearly in the100-nm-wide spectral region shown there. Physically speaking, the ZNW affects the RIFS of solitons, and it is the Raman soliton that drags the DW along with it. Note that, for a conventional PCF, λ_{DW} does not change as long as dispersion of the fiber remains the same.

One may wonder how far the linear variation seen in Fig. 8 (a) persists. To answer this question, we varied the ZNW over a much wider spectral range by modifying the Kerr nonlinearity through the filling factor of silver nanoparticles, and the results are shown in Fig 8 (b). The plot indicates that λ_{DW} increases initially in a linear fashion, but soon saturates and almost stops increasing after λ_{ZNW} exceeds 2000 nm. This saturation region is also predicted analytically (circles in fig. 8 (b)). The reason for this behavior is not difficult to understand. If we push the ZNW far away from the input wavelength, there is less chance that the spectrum of Raman soliton will approach the ZNW. However, we found that, if the doped fiber has a negative constant value equal to $\gamma_{0eff}(\omega_0)$, i.e. no ZNW exists, then λ_{DW} is close to 1275 nm, as indicated by the horizontal line in Fig. 8 (b). This suggests that the ZNW affects the DW even when it is far from the input wavelength. It seems that λ_{DW} will merge to actual DW wavelength (1275 nm) asymptotically only in the limit $\lambda_{ZNW} \to \infty$. In Fig. 8 (c) we used the filling factor f for tailoring the location of the ZNW. Fig. 8 (c) shows the variation of ZNW with the filling factor in the range $0 < f < 0.1$.

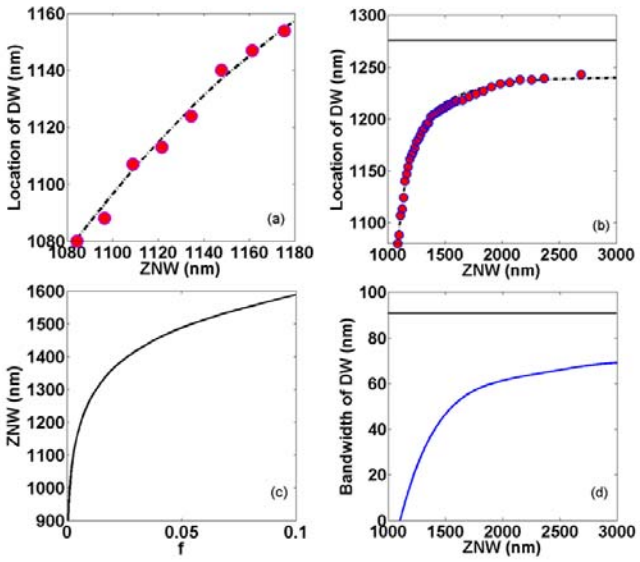

FIG. 8. (Color online) (a) Variation of DW wavelength with the ZNW both numerically (dot-dashed line) and analytically from phase-matched equation 15 (circle). (b) Same variation over a

wider range of ZNW. The horizontal line shows the wavelength of DW when ZNW does not exist. (c) Variation of ZNW with the filling factor f. (d) Variation of spectral bandwidth width of DW with the ZNW. Bandwidth is defined as the difference between the two points that are 10 dB below the peak intensity of the DW. The horizontal line shows the width of DW when ZNW does not exist.

Since the spectral bandwidth of the DW is also affected by the location of the ZNW (see Figs. 3-7), in Fig. 8(d) we show the extent of this variation. Similar to the behavior seen in Fig. 8 (b) for the central wavelength of DW, the DW bandwidth also increases rapidly initially with an increasing ZNW, but then saturates at a value of about 70 nm. Indeed, the DW bandwidth is quite large in Fig. 3(a) but is reduced considerably as the ZNW moves close to ZDW in Figs. 4-7. Since energy of the DW is also reduced under these conditions, we conclude that the ZNW affects the emission of DWs if moves closer to the ZDW of a silver doped PCF.

VI. CONCLUSIONS

We have studied, for the first time to our knowledge, the role of the ZNW on the dynamics of ultrashort pulses launched into a PCF whose core has been doped with silver nanoparticles. The effective nonlinear parameter γ_{eff} in such PCFs varies rapidly with wavelength, vanishes at a specific wavelength (the ZNW), and then it becomes negative. As a result, such PCFs acquire unique nonlinear features, one of them being that solitons can exist in the normal dispersion region. Theoretically we have confirm that how this ZNW affects the pulse evolution by creating suppression to the Raman soliton. We studied numerically the propagation of femtosecond pulses in presence of ZDW and ZNW and found a number of intriguing features. Our PCF has a single ZDW, yet it shows generation of a DW through suppression of RIFS. This DW encounters anomalous dispersion but cannot form a soliton because it experiences a negative nonlinearity. The simultaneous presence of a ZNW and a ZDW, whose relative spacing can be controlled by changing the filling factor of dopants, provides a fertile ground where new optical phenomena may occur. We found that both the central wavelength and the bandwidth of the DW are affected considerably when ZNW is varied. Position of the DW is verified analytically from the phase-matched equation and it matches quite well with the simulation. In particular, the ZNW behave like a barrier that suppresses the RIFS and does not allow red shifting of a Raman soliton beyond wavelengths longer than the ZNW. We believe that the concept of ZNW is fascinating in the context of nonlinear fiber optics and is likely to open up new and promising avenues. We are in the process of fabricating a PCF doped with silver nanoparticles so that we can verify our theoretical predictions experimentally.

ACKNOWLEDGEMENTS

Work of SB is supported by CSIR 12th plan GLASSFIB project (ESC0202). Work of GPA is supported by NSF under
award ECCS-1505636. Part of the work of SKB is supported by CSIR Emeritus Scientist Scheme-21(1017)/15/EMR-II. Some part of the work of SR is supported by SERB, DST India.

[**1**] G. P. Agrawal, *Nonlinear Fiber Optics*, 5th ed. (Academic Press, 2013).
[**2**] L. F. Mollenauer and J. P. Gordon, *Solitons in Optical Fibers: Fundamentals and applications* (Elsevier, 2006).
[**3**] T. A. Birks, J. C. Knight, and P. St. J. Russell, Opt. Lett. **22**, 961 (1997).
[**4**] P. St. J. Russell, Science **299**, 358 (2003).
[**5**] J. M. Dudley, and J. R. Taylor, Nature Photon. 3, **85** (2009).
[**6**] I. Cristiani, R. Tediosi, L. Tartara, and V. Degiorgio, Opt. Exp. **12**, 124 (2004).
[**7**] S. Roy, S. K. Bhadra, and G. P. Agrawal, Phys. Rev. A **79**, 023824 (2009).
[**8**] J. M. Dudley, G. Genty, and S. Coen, Rev. Mod. Phys. **78**, 1135 (2006).
[**9**] J. P. Gordon, Opt. Lett. **11**, 662 (1986).
[**10**] D. V. Skryabin, F. Luan, J. C. Knight, P. St. J. Russell, Science **301**, 1705 (2003).
[**11**] F. Biancalana, D. V. Skryabin, and A. V. Yulin, Phys. Rev. E **70**, 016615 (2004).
[**12**] Y. Xiang, X. Dai, S. Wen, J. Guo and D. Fan, Phys. Rev. A 84, 033815 (2011).
[**13**] S. P. Stark, A. Podlipensky, and P. St. J. Russell, Phys. Rev. Lett. **106**, 083903 (2011).
[**14**] L. Liu, Q. Tian, M. Liao, D. Zhao, G. Quin, Y. Ohishi, and W. Quin, Opt. Lett. **37**, 5124 (2012).
[**15**] L. Liu, Z. Kang, Q. Li, X. Gao, M. Liao, G. Qin, L. Hu, Y. Ohishi, and W. Qin, Appl. Phys. Lett. **105**, 181113 (2014).
[**16**] R. Driben, A. Husakou, and J. Herrmann, Opt. Exp. **17**, 17989 (2009).
[**17**] R. Driben, J. Herrmann, Opt. Lett. 35, 2529 (2010).
[**18**] S. Bose, R. Chattopadhyay, S. Roy, and S. K.Bhadra, JOSA B **33**, 1014 (2016).
[**19**] J. C. M. Garnett, Philos. Trans. R. Soc. London 203, **385** (1904).

[**20**] P. B. Johnson and R. W. Christy, Phys. Rev. B **6**, 4370 (1972).
[**21**] J. E. Sipe and R. W. Boyd, Phys. Rev. A **46**, 1614 (1992).
[**22**] D. Anderson, Phys. Rev. A **27**, 3135 (1983).
[**23**] N. Akhmediev and M. Karlsson, Phys. Rev. A **51**, 2602 (1995)